Supporting Information

Advancing Scalable and Controllable Multi-Core Droplet Generation with Double Disturbance Flow Focusing

Chen Li,[a,b] Kai Mu,[a] Fangsheng Huang,*[,a,b] Zhiqiang Zhu,*[,b,c,d] Ting Si[a]

[a] Department of Modern Mechanics, University of Science and Technology of China, Hefei, Anhui 230026, China.

[b] Institute of Advanced Technology, University of Science and Technology of China, Hefei, Anhui 230088, China.

[c] Department of Precision Machinery and Precision Instrumentation, University of Science and Technology of China, Hefei, Anhui 230026, China.

[d] Key Laboratory of Precision Scientific Instrumentation of Anhui Higher Education Institutes, University of Science and Technology of China, Hefei, Anhui 230026, China.

*Corresponding authors

*E-mail: huangfs@ustc.edu.cn.

*E-mail: zqzhu2017@ustc.edu.cn.

1. Supporting Figures

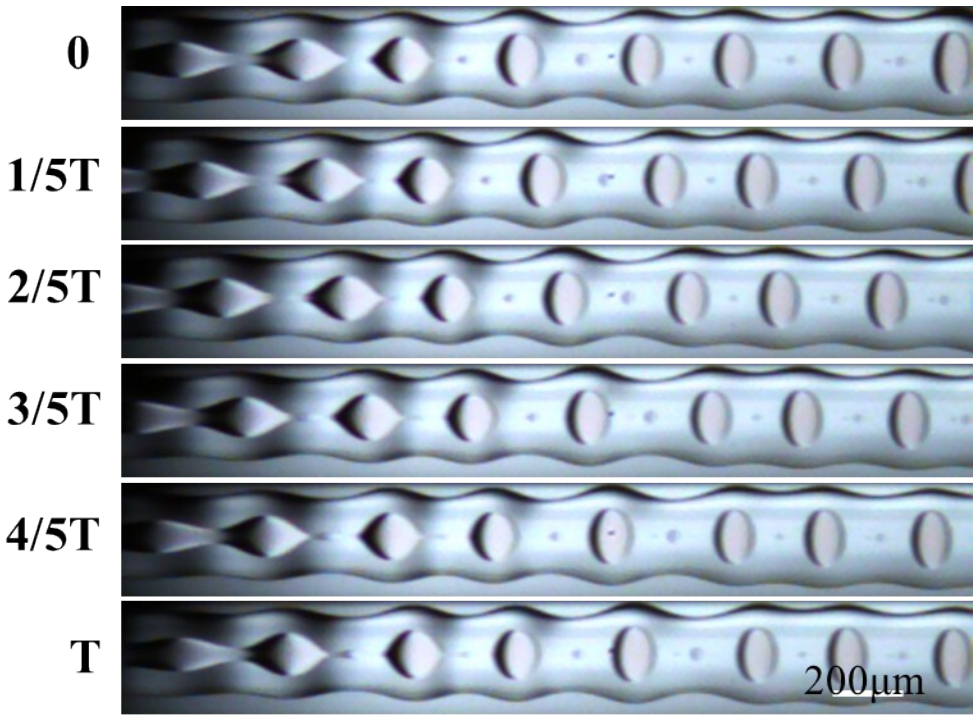

Figure S1 Image sequence showing one cycle of the inner jet break up.

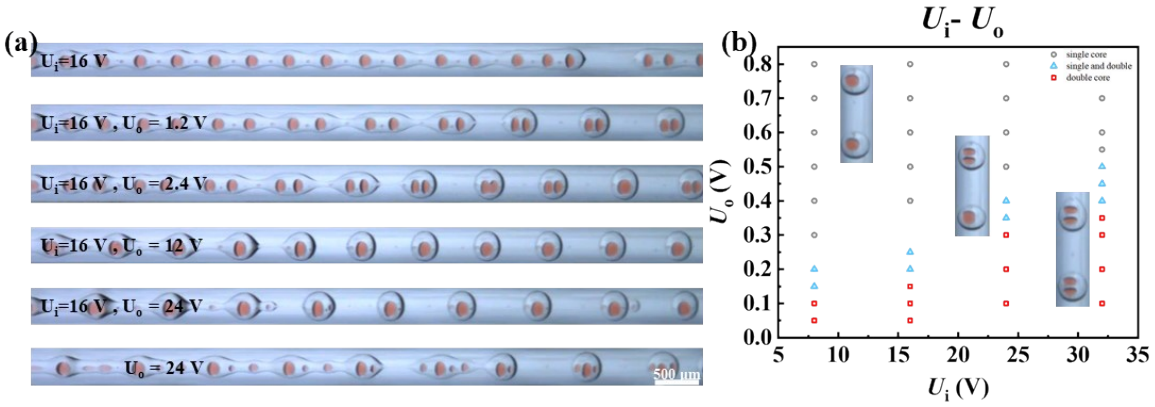

Figure S2 Droplet fusion generates single core droplets, the jet break up while f_i = 6000 Hz, f_o = 3000 Hz.

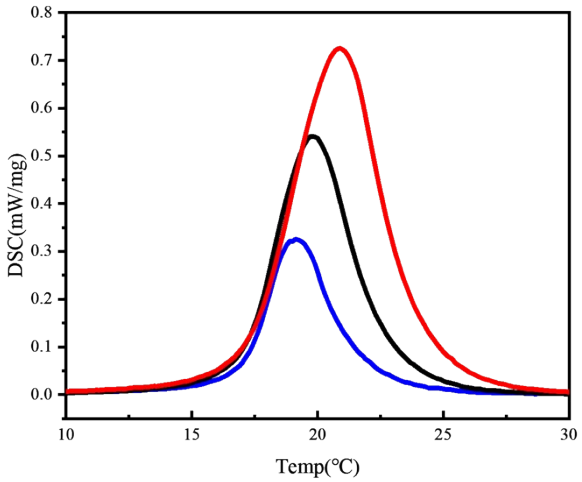

Figure S3 Thermal performance of PCM microcapsules.

2. Supporting Table

	Q_o-Q_i (mL/h)	f_i (kHz)	f_o (kHz)	T_0 (℃)	T_1 (℃)	T_2 (℃)	ΔH_m(J/g)
1	95-5	9.6	4.8	16.9	19.1	21.7	7.543
2	45-5	4.8	2.4	16.9	19.7	22.9	13.59
3	43-7	4.8	2.4	17.2	20.9	24.1	21.18

Table R1 Parameters of PCM microcapsules.

3. Supporting analysis

Droplet formation is associated with disturbances in jet interfaces, which are influenced by factors such as fluid viscosity, interfacial tension, and flow velocity. Instability theory, a well-established tool for analyzing disturbance growth, quantifies growth rates and wavelengths, and identifies the impacts of parameters. Linear stability theory is commonly employed to study jet instability and breakup. This section, building on previous research, develops a simplified theoretical model based on coaxial flow focusing experiments, focusing primarily on the temporal stability analysis of a three-phase 'water-oil-water' composite jet, and investigates the effects of key dimensionless parameters on jet stability.

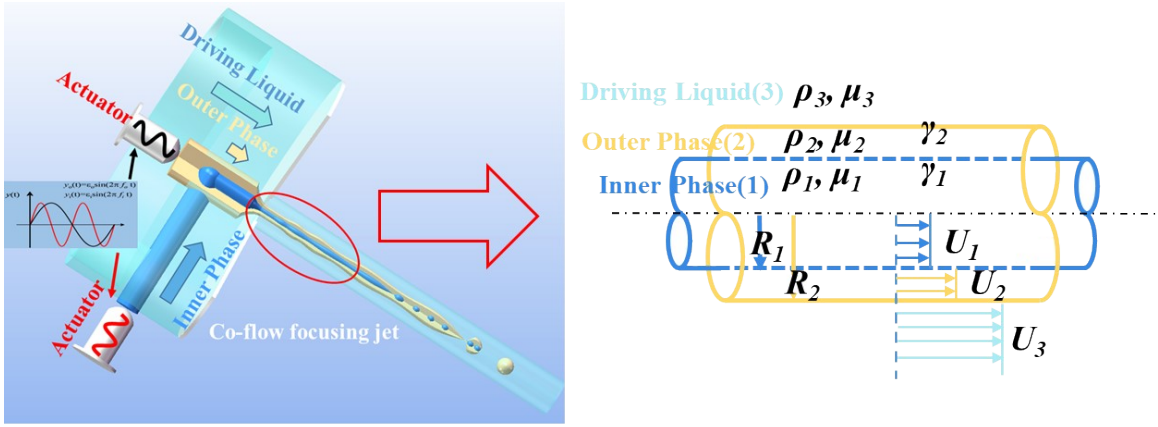

Figure S4 Schematic diagram of coaxial jet physical model.

The physical parameters involved in the composite jet model are: the density $\rho_{1,2,3}$ of the inner and outer jets and the driving fluid, the kinetic viscosity coefficients $\mu_{1,2,3}$ the basic velocity $U_{1,2,3}$(r), the fluid flow rate $Q_{1,2,3}$, the interfacial tension coefficients of the inner and outer layers $\gamma_{1,2}$, and the radii of the inner and outer jets $R_{1,2}$, etc. (the subscripts 1,2,3 stand for the inner and outer jets, respectively, as well as the driving fluid). The schematic of the physical model of a coaxial jet is illustrated in **Figure S4.** The physical quantities of the outer jet are selected as the characteristic scales, including its radius R_2, mean velocity $U_2 = Q_2/\pi(R_2^2 - R_1^2)$, density ρ_2, viscosity coefficient μ_2,

and interfacial tension coefficient γ_2; the corresponding characteristic time is $R_2/\bar{U}_2$, and the characteristic pressure is $\rho_2\bar{U}_2^2$. Dimensionless parameters are involved, such as: the Reynolds number $Re = \rho_2\bar{U}_2R_2/\mu_2$, and the Weber's number $We = \rho_2\bar{U}_2^2R_2/\gamma_2$, density ratios $S = \rho_1/\rho_2$ and $Q = \rho_3/\rho_2$, viscosity ratios $N = \mu_1/\mu_2$ and $M = \mu_3/\mu_2$, radius ratio of the inner and outer layers of the jet $r_Q = R_1/R_2$, and ratio of the internal and external interfacial tension coefficient $\tau = \gamma_1/\gamma_2$.

The specific linear stability analysis procedure can be referred to the previous work of our group[1].

The relationship between the dimensionless disturbance growth rate β and the wave number α under different parameter stretching modes is given by calculation.

Taking the basic working condition as an example, the internal phase is 0.2 wt% PVA aqueous solution with a flow rate of 10 mL/h; the external phase is added with 2 wt% DC749 silicone oil solution, 90 mL/h; the driving pure water, 1116 mL/h, and the diameter of the focusing small holes is 450 μm; the calculations give: $r_Q = 0.32$, $\tau = 0.58$, $N = 0.015$, $M = 0.0157$, $S = 1.033$, $Q = 1.031$, $Re = 2.357$, $We = 12.549$.

Under the given parameters, each α−β curve, derived from the dispersion relation $\beta = \beta(\alpha)$ exhibits a maximum perturbation growth rate β_{max}, its corresponding axial wavenumber α_{max}, and a critical wavenumber α_{cut}. The wavenumber α_{cut} corresponds to the point where the β−α curve intersects the abscissa, as illustrated in **Figure S5**. For values of α less than α_{cut}, the perturbation growth rate β is positive, meaning the size of α_{cut} determines the extent of the unstable region (the upper limit of the synchronization interval). Since the perturbation growth rate at β_{max} is faster than at other wavenumbers, it is generally considered to play a decisive role in the temporal stability of the jet and ultimately governs jet breakup. The corresponding wavenumber α_{max} represents the natural breakup frequency and determines the size of the droplets formed after jet disintegration.

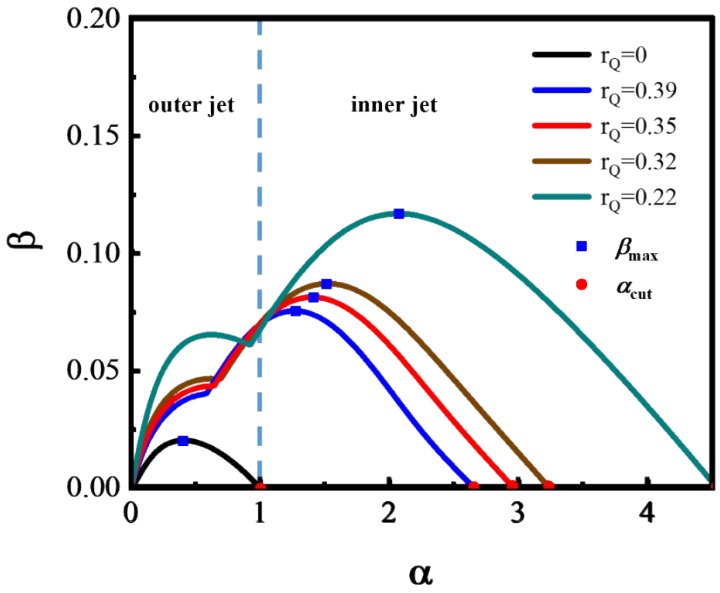

Figure S5 Perturbation growth rate-wave number of the coaxial jet.

When the internal and external phase flow rates are fixed, and only the flow ratio between the internal and external phases is varied while keeping the total flow rate constant ($Q_i + Q_o$), we calculate the perturbation growth rates using both the uniaxial jet model and the coaxial jet model. Specifically, we compare the wavenumber growth rate diagrams for the coaxial jet with and without coupling effects. The schematic diagram and corresponding calculation results are presented in **Figure S5**.

In a typical weak coupling region ($r_Q \leq 0.4$), as r_Q increases, the α_{max} of the internal jet decreases, and the frequency of natural jet fragmentation to generate droplets decreases; α_{cut} decreases, and the upper limit of the synchronization interval decreases; the final generated droplet core becomes larger; The α_{max} of the outer jet decreases, and the outer droplet size increases and the number of kernels becomes larger in the case of natural fragmentation. As previously demonstrated, with the gradual increase of r_Q, the rupture length of the external jet decreases, indicating that the presence of the internal interface significantly promotes the early decomposition of the external interface. In other words, the rupture of the internal jet and the resulting droplets result in substantial alterations to capillary pressure, exerting a considerable influence on the disturbance of the external jet surface and consequently modifying the rupture time.[1, 2]

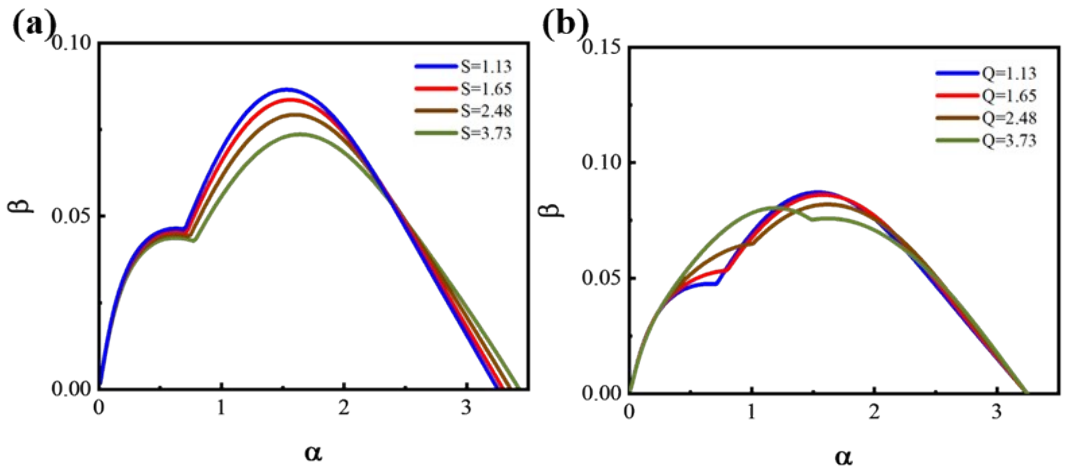

Figure S6(a) Effect of inner layer fluid density on the stability of coaxial jet. **(b)** Effect of driving fluid density on the stability of coaxial jet.

We further investigated the effect of inner layer fluid and driving fluid density on the coaxial jet stability. As shown in **Figure S6**, the disturbance growth rate of the inner jet decreases with the increase of the density ratios S (inner/outer) and Q (driven/outer), and the densities of the inner and driven fluids both contribute to the stability of the coaxial jet; a comparison of the effects of S and Q also reveals that β is more sensitive to the change of S. The density of the inner and driven fluids on the stability of the coaxial jet is also shown in **Figure S6**, which shows that the density ratio S (inner/outer) is very high. The effect of density on the stability of the coaxial jet mainly stems from the change of jet inertia: when increasing S, the inertia of the coaxial jet is increased, but the interfacial tension and viscous shear force on the jet are kept constant at this time, so the growth rate of the perturbation will be slower. In addition, increasing S also causes the maximum perturbation growth rate β_{max} corresponding to α_{max} and the cutoff wave number α_{cut} of the internal-phase jet to increase with S, which means that the natural breakup frequency of the internal-phase jet and the upper limit of the synchronization interval increase.

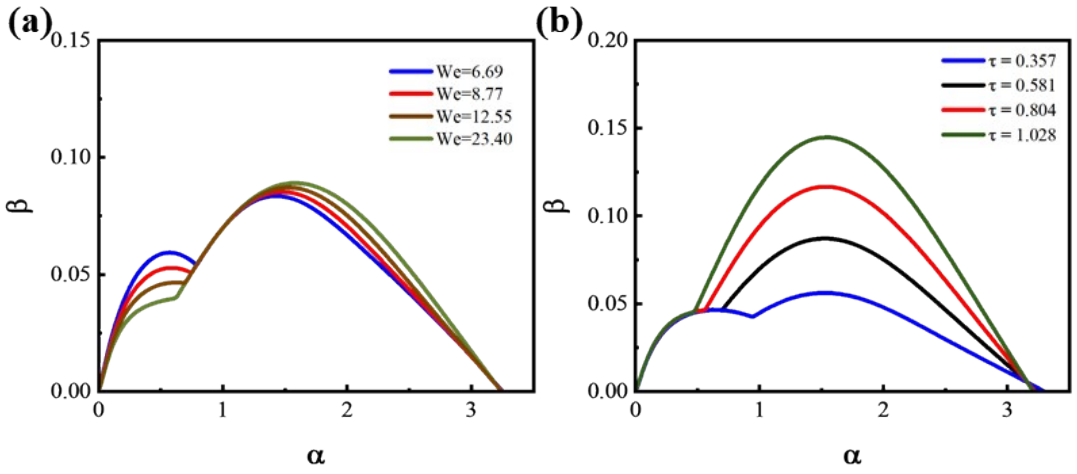

Figure S7(a) Weber number We and the effect on the perturbation growth rate β. **(b)** Effect of the interfacial tension γ_1 ($\tau = \gamma_1/\gamma_2$) between the inner and outer phase fluids on the perturbation growth rate β.

In order to ascertain the impact of interfacial tension on jet stability, we conducted a series of calculations, varying solely the inner layer interfacial tension γ_2 ($We = \rho_2 U_2^2 R_2/\gamma_2$) and the outer layer interfacial tension γ_1 ($\tau = \gamma_1/\gamma_2$) to determine their effect on the perturbation growth rate β.

As illustrated in **Figure S7**(a), when solely the interfacial tension of phase 2.3 is altered for a fixed flow parameter, thereby modifying the Weber number We, it is evident that an increase in the outer interfacial tension results in a reduction in We, which corresponds to an increase in the maximum perturbation growth rate. As a result, the outer jet becomes more unstable, while the perturbation growth rate of the inner jet is reduced. The cutoff wave number of the inner jet, α_{cut}, remains unchanged, indicating that the upper limit of the synchronization interval of the inner-phase jet is unaltered.

Conversely, the maximum perturbation growth rate β_{imax} of the inner jet increases with τ, indicating that the interfacial tension in the inner layer facilitates jet fragmentation. In general, an increase in interfacial tension at both the inner and outer interfaces results in enhanced jet fragmentation, although this has a relatively limited impact on the fragmentation wavelength and stability region of the coaxial jet.

Furthermore, in order to ascertain the impact of the viscosity of each phase fluid on jet stability, we calculated the effect of modifying solely the viscosity μ_1 of the inner-phase fluid ($N = \mu_1/\mu_2$), the viscosity μ_2 of the outer-phase fluid ($Re = \rho_2 U_2 R_2/\mu_2$) and the viscosity μ_3 of the driving-phase fluid ($M = \mu_3/\mu_2$) on the perturbation growth rate β was also investigated, as illustrated in **Figure S8.**

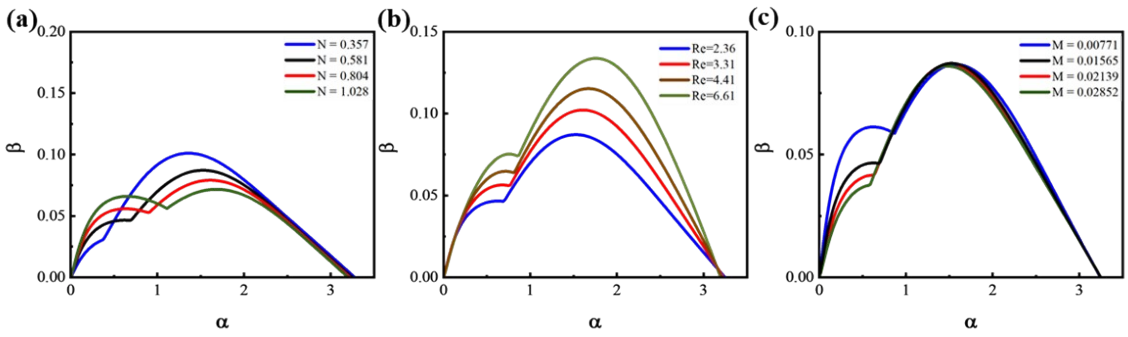

Figure S8(a) Effect of viscosity μ_1 ($N = \mu_1/\mu_2$) of the internal-phase fluid on the perturbation growth rate β. **(b)** Reynolds number Re and the effect on the perturbation growth rate β. **(c)** Effect of viscosity μ_3 ($M = \mu_3/\mu_2$) of the driving-phase fluid on the perturbation growth rate β.

As Re decreases or N and M increase, the most unsteady perturbation growth rate β_{max} decreases, which indicates that the viscosity of the fluid can inhibit the destabilization of the coaxial jet. This is because increasing the viscosity of the fluid will increase the viscous drag and viscous dissipation effect, making the disturbance decay faster. At this time, the maximum perturbation growth rate β_{max} of the internal jet corresponds to the decrease of αmax, that is, the natural breakup frequency of the internal jet decreases, while the cutoff wave number α_{cut} is almost unchanged, i.e., the upper limit of the synchronization interval remains unchanged.

To evaluate the mechanical buffering effect of capsules with different core sizes, we prepared microcapsules with consistent particle sizes but varying core sizes by encapsulating a PVA aqueous solution within ETPTA. The flow rates for each group were set at 8-112 mL/h, 12-108 mL/h, 20-100 mL/h, and 30-90 mL/h, as illustrated in **Figure S9(a)**. After repeated washing with water, the obtained capsules were placed in

an oven and dried at 50℃ for 24 hours. We maintained a ratio of 2.5 mL of capsules to 1.25 g of a 2 wt% sodium alginate solution, ensuring the capsules and solution were evenly mixed in the mold, as shown in **Figure S9(b)**. (To expedite drying, the base was made of glass instead of acrylic, which differs from the experiment described in the main text. Additionally, the 30-90 mL/h combination does not belong to the weak coupling mode and is included here solely for comparison.)

A small steel ball, with a diameter of 7 mm and a mass of 1.4 g, was dropped freely from a height of 8 cm above the mold. A high-speed camera recorded the peak height of the ball's rebound, reflecting the gravitational potential energy stored after impact. As shown in **Figure S9(c)**, the ball rebounded the highest after colliding with the capsules generated at the flow rate of 8-112 mL/h, indicating weaker buffering and energy absorption effects. In multiple experiments, the average rebound height for the combination capsule impacted by the ball at a flow rate of 8-112 mL/h was the highest at 35.1 mm, followed by the 12-108 mL/h capsules at 31.8 mm. Conversely, the 20-100 mL/h combination capsules exhibited a higher proportion of inner core, while the 30-90 mL/h combination microcapsules demonstrated the best energy absorption effect, with rebound heights of 25.4 mm and 23.2 mm, respectively.

These experiments indicate that, within a certain proportion, larger core sizes yield enhanced energy absorption through deformation.

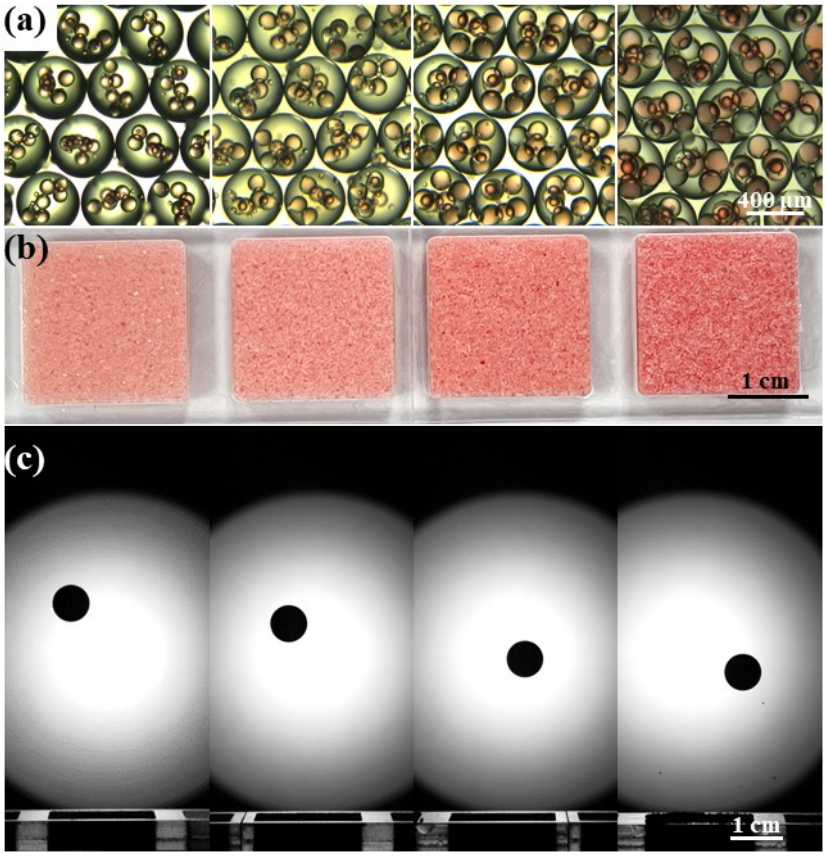

Figure S9 The mechanical buffering effect of capsules with different core sizes. **(a)** Microscopic images of six-core microcapsules obtained with flow rate of 8-112 mL/h, 12-108 mL/h, 20-100 mL/h, and 30-90 mL/h. **(b)** After complete dehydration, the capsules are mixed with sodium alginate solution and filled into an acrylic board. The overall microcapsule block is obtained after drying, and its buffering effect is tested. **(c)** High-speed camera recorded photos showing a small steel ball with a diameter of 7 mm freely released from a height of 8 cm, impacting the microcapsule blocks, with the highest rebound height recorded.

4. Supporting Videos

Video S1 High-speed photography of the jet breakup phenomenon when the inner and outer jets are in a state of strong coupling.

Video S2 The video of droplet generation for outer-phase excitation frequencies at 1/2,

1/3, 1/4, and 1/5 of the inner-phase excitation frequency.

Video S3 Single-core double emulsion microcapsules were obtained through droplet fusion, with a large difference in internal and external flow rates.

Video S4 The video demonstrating the buffering and energy absorption effect of multi-core microcapsules.

Reference

1. K. Mu, G. Li and T. Si, *Physics of Fluids*, 2020, **32**, 092107.
2. K. Mu, H. Ding and T. Si, *Physics of Fluids*, 2020, **32**, 042103.